Local trigonal modes and the suppression of the charge density wave in TiSe_{2−x}Te_{x}

A. Wegner, D. Louca, and J. Yang

Phys. Rev. B **99**, 205110 — Published 9 May 2019

DOI: 10.1103/PhysRevB.99.205110

Local trigonal modes and the suppression of the charge density wave in $TiSe_{2-x}Te_x$

A. Wegner and D. Louca
Department of Physics, University of Virginia, Charlottesville, Virginia 22904

J. Yang
Department of Physics, Central Michigan University, Mount Pleasant, Michigan 48859 22904

(Dated: April 19, 2019)

The composition dependence of the charge density wave (CDW) state is investigated in the solid solution of 1T-$TiSe_{2-x}Te_2$ using neutron scattering and the pair density function analysis. It is observed that the CDW order is quickly suppressed with doping, between $0.2 \leq x \leq 0.25$. The suppression of the CDW is coupled with a change in the local symmetry from hexagonal to monoclinic. In the monoclinic, high temperature phase, a Jahn-Teller (JT) distortion is observed between Ti and Se bonds that is suppressed with Te doping. These observations favor a CDW that is driven by a cooperative JT effect as Ti-Se bond shortening is crucial to CDW formation and excess chalcogen to Ti charge transfer inhibits the JT mechanism.

I. INTRODUCTION

The transition metal dichalcogenides (TMD) are quasi-two dimensional layered materials that exhibit many interesting electronic properties from topological Weyl semimetals[1] to quantum spin liquids[2]. A notable property common to many TMD materials is a charge density wave (CDW) ordering. CDWs frequently occur in proximity to other interesting phenomena, such as superconductivity, in materials with competing order. TMDs such as $TiSe_2$ exhibit prototypical CDW transitions that allow the CDW transition to be studied decoupled from other phenomena. CDWs occur in many polytypes, such as the octohedral 1T and trigonal prismatic 2H, in which the number refers to the number of monolayers in the unit cell and the letter refers to the local coordination of the transition metal atom. 1T-$TiSe_2$ has been extensively studied for its charge density wave (CDW) transition occurring upon cooling below 200 K[3]. The mechanism driving this transition is still controversial despite years of research, with exciton condensation[4] and a pseudo-Jahn Teller (JT) effect[5] proposed as candidate processes driving the CDW order.The layered structure makes 1T-$TiSe_2$ a good candidate for thin film applications[6–9]. Furthermore, superconductivity has been discovered at CDW domain walls under pressure,[10] with the intercalation of Cu[11] or substitution of Ti with Ta or Pd.[12,13] More recently, $TiSe_2$ has been proposed as a cathode material for Mg ion batteries[14], spurring an increase in interest in the CDW order and revitalizing the effort to understand this phase transition[15–18]. Using a combination of angle-resolved photoemission spectroscopy (ARPES) and neutron scattering on pristine $TiSe_2$, we proposed that a JT mechanism associated with local symmetry breaking in the low temperature phase is necessary to describe the CDW[19]. On the other end of the phase diagram, $TiTe_2$ does not exhibit a CDW transition for reasons that have not been explored. How the CDW disappears as a function of x in $TiSe_{2-x}Te_x$ has not been investigated. While it is to be expected that Te doping will eventually suppress the CDW transition, a study of the solid solution with doping can provide insight to what happens to the lattice with doping. Understanding how the lattice changes between the CDW forming members of the doping series and the non-CDW forming members is important to uncovering the lattice effects of CDW formation.

Both 1T-$TiSe_2$ and $TiTe_2$ crystallize in the CdI-type structure. The structure consists of a hexagonal lattice of Ti atoms surrounded by chalcogen atoms in a trigonally distorted octahedral environment (Fig 1a). The TiX_6 (X=Se, Te) octahedra are arranged in X-Ti-X layers that are held together by Van der Waals forces[20]. The CDW phase of the 1T-$TiSe_2$ is a triple q state formed by wave vectors $\vec{q}_1 = (\frac{1}{2}, 0, \frac{1}{2})$, $\vec{q}_2 = (0, \overline{\frac{1}{2}}, \frac{1}{2})$, and $\vec{q}_3 = (\overline{\frac{1}{2}}, \frac{1}{2}, \frac{1}{2})$. The electronic character of $TiSe_2$ is a semimetal with a negligible gap, with a hole pocket from the Se 4p band at the Γ point of the Brillouin Zone (BZ) and electron pockets from the Ti 3d bands at M[21]. $TiTe_2$ is a semimetal with an indirect gap of 0.6 eV between the Te 5p and Ti 3d bands[22,23]. In this paper we present results from neutron scattering experiments of solid solutions of $TiSe_{2-x}Te_x$ that show the CDW transition is suppressed between $0.2 \leq x \leq 0.25$ Using the pair density function (PDF) analysis we observe changes in the local structure that persist above the CDW transition temperature (T_{CDW}), with atomic distortions indicative of a JT distortion and we present a phase diagram showing that the CDW transition vanishes between $0.2 \leq x \leq 0.25$ as Te is doped into $TiSe_2$. We also observe how the trigonal distortions associated with the CDW phase are suppressed with Te doping. It is suggested that Te doping inhibits a cooperative JT effect, which suppresses the CDW phase.

II. EXPERIMENT

Powder samples were prepared by the solid state reaction method by mixing elemental Ti, Se, and Te. The powders were pelletized and sealed in a quartz tube and

heated to 800 °C for 48 hours and slowly cooled to room temperature. They were ground and pelletized for a second time before sintering under the same conditions to increase phase homogeneity. Samples of $TiSe_{2-x}Te_x$ were prepared for x = 0 (pristine $TiSe_2$,) 0.025, 0.05, 0.1, 0.2, 0.25, 0.3, 0.5, 1, and 2 (pristine $TiTe_2$). Experiments were conducted using the constant wavelength diffractometers, BT-1 at the NIST Center for Neutron Research (NCNR) and HB-2A at the High Flux Isotope Reactor (HFIR) at Oak Ridge National Laboratory (ORNL). The wavelengths used for the measurements were $\lambda = 1.540$ Å (Cu 311) at NCNR and $\lambda = 1.539$ Å (Ge 115) at HFIR. Further measurements were carried out at the time-of-flight neutron diffractometer, the Nanoscale Ordered Materials Diffractometer (NOMAD) at the Spallation Neutron Source (SNS) of ORNL. NOMAD is a diffractometer with a large bandwidth of momentum transfer, Q, and provides the total structure function S(Q). The S(Q) was Fourier transformed into real space to provide the PDF[24]. The PDF is a real space representation of the atomic correlations and does not assume any lattice periodicity. For the Fourier transform of this data, we used a maximum Q of 40 $Å^{-1}$.

The PDF analysis is a powerful tool for analyzing the local atomic structure and takes diffuse scattering into account. It is obtained after the sample environment and empty vanadium can are subtracted from the S(Q) and the data is normalized by a vanadium rod. The PDF is a function that contains information about the distribution of distances between atoms in the unit cell and is defined as:

$$G(r)_{\rm exp} = \frac{2}{\pi}\int_0^\infty Q[S(Q)-1]sin(Qr)dQ$$

A model G(r) can be calculated from the atomic coordinates and unit cell dimensions of the crystal model to obtain:

$$G(r)_{\rm mod} = \frac{1}{r}\sum_i\sum_j \frac{b_i b_j}{<b>^2}\delta(r-r_{ij}) - 4\pi\rho_0$$

where b_i is the scattering length for atom i and ρ_o is the atomic density of the crystal. The model $G(r)_{\rm mod}$ is refined to fit the experimental $G(r)_{\rm exp}$ when differences are observed.

III. AVERAGE STRUCTURE

We first begin by describing the average structure. In Fig 1(b), the diffraction pattern is shown as a function of temperature for the x = 0 system. Earlier studies reported the high temperature phase of x = 0 to be hexagonal with space group $P\bar{3}m1$ and lattice constants a = b = 3.537 ± 0.003 Å and c = 6.00 ± 0.030 Å[25]. Below

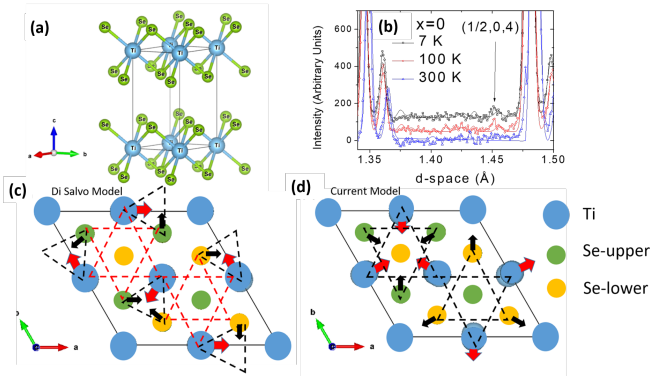

FIG. 1. (a) The unit cell for the undistorted hexagonal phase at high temperature. (b) A temperature dependent superlattice peak appears below T_{CDW} in the $TiSe_2$ sample. A comparison of the breathing mode (c) unit cell consistent with the local structure and the rotation mode (d) distortions that have been previously reported.

200 K, the CDW state forms and a 2 x 2 x 2 superlattice peak appears while the symmetry changes to $P\bar{3}c1$. The reported crystal structure modulation that leads to the CDW is the one by Di Salvo et al[3] which consists of a rotational distortion and displacements of 0.014 ± 0.003 Å and 0.042 ± 0.007 Å of the Se and Ti atoms, respectively, around the Star of David motif. Given that the Te distortion is larger than the Se distortion the Star of David becomes distorted. The result of the distortion is the creation of $TiSe_2$ trimers with slightly shortened bonds[3] as shown in Fig. 1(c).

Superlattice peaks at half-integer (hkl) indices of the primitive hexagonal unit cell are observed (Fig 1b). The CDW distortion is small, thus the intensity of the CDW peaks are of the order of 1% of the non-CDW peaks, which is comparable to the intensity of the reflections reported from single crystal diffraction[3]. The superlattice peaks are similar in intensity to the peaks arising from impurities such as elemental Ti, Se, and Te, hence a superlattice reflection is shown with a 2θ that does not coincide with reflections from the extra phases. Fig. 1(b) shows the temperature dependence of the $(\frac{1}{2}, 0, 4)$ peak in $TiSe_2$. The diffraction data are fit using the reported symmetries of $P\bar{3}c1$ at 7 and 100 K and $P\bar{3}m1$ at 300 K with $\chi^2 = 3.57$, 3.49, and 4.43, respectively.

Upon doping, the low temperature symmetry remains unchanged but the CDW transition is quickly suppressed. Shown in Fig. 2(a) is a plot of the diffraction patterns at two temperatures for x = 0.2. Evidence for the commensurate CDW order is observed in this composition as well, but by x = 0.25, shown in Fig 2(b), the CDW transition is suppressed.

As the x increases as seen in the nominally x = 1 sample the low temperature crystal symmetry deviates from the hexagonal lattice of $TiSe_2$. At low d-spacing shoulders appear on Bragg peaks as seen in the expanded range

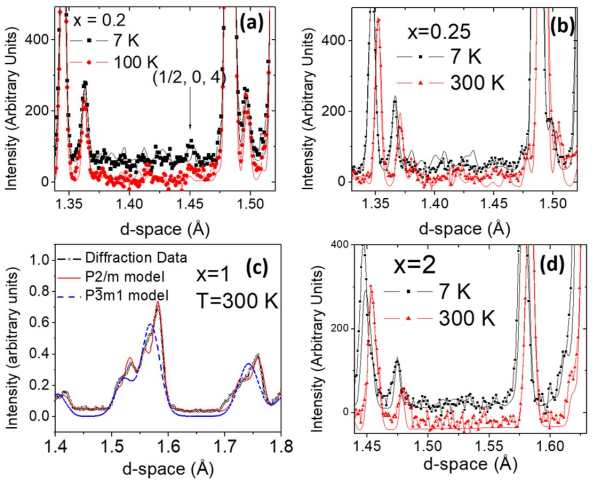

FIG. 2. (a) As Te is doped into the system the superlattice peak still appears with x = 0.2. (b) At x = 0.25 the superalattice peak is no longer present and the CDW has been suppressed. (c) At x = 1 shoulders appear on peaks in the diffraction pattern due to a monoclinic local structure. (d) The superlattice peak does not appear at the Te end of the doping spectrum.

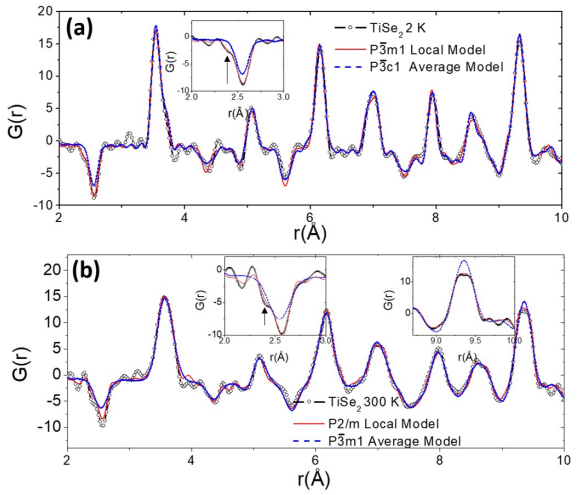

FIG. 3. (a) The local structure of $TiSe_2$ in the low temperature CDW phase is fit with the previously reported P$\bar{3}$c1 model and with a P$\bar{3}$m1 model. Both fit long range correlations well but only the P$\bar{3}$m1 model can reproduce splitting of the first peak. (b) The high temperature phase local structure is fit with the hexagonal average structure and with a monoclinic model. Only the monoclinic model can reproduce correlations above 9 Å.

of the diffraction data in Fig. 2(c) that are indicative of a monoclinic distortion. The diffraction patterns for x = 1 can be fit using the symmetry P2/m with $\chi^2 = 4.881$. Refinement of occupancy of Se and Te suggests that the stoichiometry is closer to x = .6, although the unit cell size agrees with the literature[26]. No CDW is observed and the material does not show a structural phase transition upon warming. At x = 2, in $TiTe_2$, no CDW peaks are observed either (Fig. 2(d)), consistent with the average structure reported in previous studies of $TiTe_2$.

IV. LOCAL STRUCTURE

The observed CDW peaks cannot be uniquely described by the P$\bar{3}$c1 symmetry, however. As we recently found, a superlattice with identical lattice constants and distortions described using P$\bar{3}m1$ symmetry fits the average structure of $TiSe_2$ as well, while improving the fit of the local distortions[19]. The $P\bar{3}m1$ symmetry contains a breathing mode distortion while the $P\bar{3}c1$ symmetry contains a rotational distortion. Local analysis must be employed to see how the distortions occur in the solid solution. Shown in Fig. 2 is the G(r) corresponding to the local atomic structure of $TiSe_2$ at (a) 2 K and (b) 300 K. The negative Ti-Se correlation peak at 2.55 Å has a shoulder to the left at 2.41 Å. The magnitude of the split is not temperature dependent but the intensity is. This is shown in the insets of Fig 3. The $P\bar{3}c1$ CDW model of Di Salvo fits the local structure of the 2 K data well except for the first Ti-Se peak. This is seen in Fig 2(a) and in the inset. While the distortions associated with the CDW phase lead to shortened Se-Ti-Se trimers as seen in Fig 1(c), the bonds are only shortened by 0.06 Å which is not nearly enough to reflect the distortion in the local strucutre. However, when the symmetry constraints are relaxed to $P\bar{3}m1$ the first peak can be fit well as seen in the figure. This is because in this symmetry, the constraints of the atom displacements are lifted and the Ti atoms move to form a breathing mode, rather than Ti atoms being constrained to move along the **a** or **b** axis toward another Ti atom as in the $P\bar{3}c1$ symmetry, where **a** and **b** are the lattice vectors of the primitive hexagonal unit cell. With $P\bar{3}m1$ symmetry, Ti atoms move toward Se atoms with a JT-like breathing distortion, shown in Fig. 1(d) in comparison to the Di Salvo model in Fig. 1(a) and fits the local structure very well. This breathing distortion shortens the bonds of $\frac{1}{8}$ Ti-Se nearest neighbor bonds as six of the eight Ti atoms in the unit cell move toward one of their six neighbors. In the non-CDW phase, above 200 K,the distortions are is still present. At high temperatures, the long range correlations of the PDF cannot be fit with the hexagonal symmetry $P\bar{3}m1$ despite the good fit of the average structure using this symmetry. A local monoclinic model improves the fit as shown in Fig 3(b). At long distances of r > 9 Å above T_{CDW}, peaks corresponding to correlations two unit cells away split into separate distinct peaks (see inset of Fig. 3(b).

At x = 0.1, the splitting of the first Ti-Se peak is unchanged, as shown in Fig. 4(a-b). The peak at 2.55 Å has a shoulder at 2.41 Å for x $\leq$ 0.1. The concentration of Te is too low to observe a separate Ti-Te pair correlation.

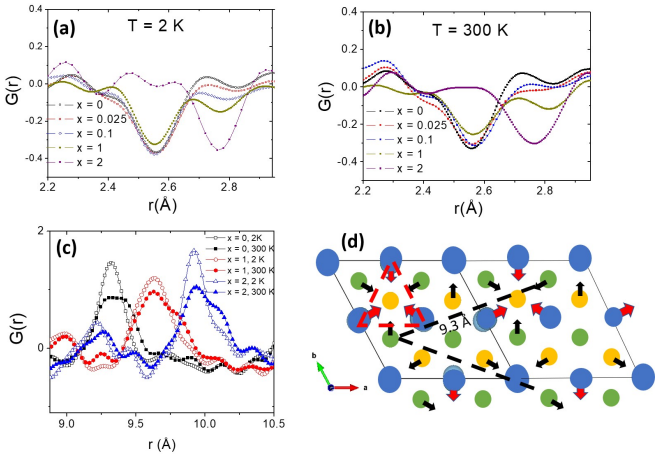

FIG. 4. (a) The composition dependence of the first Ti-Se and Ti-Te peak at 2 K showing that at low concentrations a shoulder appears on the first peak that is not present in the x = 1 and x = 2 samples. (b) The composition dependence of the first Ti-Se and Ti-Te peak at 300 K shows that the splitting of the first peak occurs even above the T_{CDW} (c) PDF above 9 Å shows that at high temperatures the long distance correlations become split as a monoclinic distortion breaks the a = b axis symmetry. (d) The red dashed lines show the triangles of Ti that shift toward Se to cause the distortion observed in (a) and (b). The black dashed lines indicate correlations of 9.3 Å that, along with symmetry equivalent correlations outside the plotted region, make up the peak that is shown in (c).

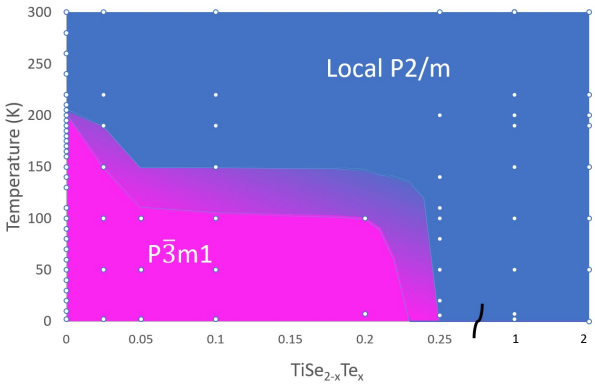

FIG. 5. Phase diagram for the $TiSe_{2-x}Te_x$ system. The CDW transition is suppressed with Te doping and does not appear above a Te concentration of 12.5%.

At high temperature the peak is more apparent because the shoulder peak is sharper while the main peak becomes broader. At correlations larger than 9 Å, there is a significant change above the T_{CDW}. Most notably, the peak at 9.34 Å (Fig 4(c)) splits into two. This splitting can be fit using a monoclinic symmetry with space group P2/m. The temperature at which this splitting occurs decreases as the concentration of Te is increased. This peak is primarily composed of Se-Se correlations. The correlations are made up of Se atoms that are separated by a translation of $2\mathbf{a} - \mathbf{b}$ and all symmetry equivalents. Fig. 4(d) shows two of the correlations that split due to the high temperature monoclinic distortion that breaks the a = b symmetry.

The G(r) of the x = 1 sample fits the monoclinic phase with a = 25.004 ± 0.011 Å b = 11.0072 ± 0.0041 Å c = 12.6097 ± 0.0071 Å β = 88.752 ± 0.057 observed in the average structure. As the Se and Te atoms are different sizes, separate peaks occur at 2.55 and 2.79 Å corresponding to Ti-Se and Ti-Te nearest neighbor peaks, respectively. Integration of the peaks at 2.55 and 2.79 Å suggests that the stoichiometry of the sample is closer to x = 0.65. The peaks at 2.55 and 2.79 Å are symmetric and there is no evidence for the JT distortion observed in the CDW materials. For x = 2, there is no splitting of the nearest neighbor Ti-Te peak at 2.8 Å and no JT distortion is observed in the local structure. As a function of temperature the local trigonal symmetry is broken as in the high temperature phase of the doping series.

The results indicate that the JT distortion exists above T_{CDW} and becomes cooperative when the CDW forms. This model retains the breathing mode distortions with the same bond lengths as the CDW phase while breaking the overall local trigonal symmetry.

V. DISCUSSION

The composition dependence of the CDW order is shown in the phase diagram of Fig. 5. It is clear that as Te is doped into the system, the CDW transition is suppressed. For x = 0.025, T_{CDW} is between 150 and 190 K. For x = 0.1 transition occurs between 100 and 150 K. From the presence of superlattice peaks, the highest doping level to undergo the CDW transtion is x = 0.2 while the absence of superlattice reflections in x = 0.25 and x = 0.3 correspond to the absence of the CDW order.

Splitting of the first Ti-Se peak associated with a trigonal distortion is clearly observed in the local structure for samples with a CDW phase. This splitting does not occur when the concentration of Te is high enough that the CDW is suppressed. As this splitting occurs even at high temperatures, well above the T_{CDW}, there is a clear connection between the distortions and CDW formation. The magnitude of the Ti-Se distortion and the percentage of bonds distorted remains constant for small x despite a decrease in T_{CDW}. It is likely that competition between disorder introduced by Te and tendency toward a long range cooperative JT order with Se leads to a lowering of the transition temperature.

As mentioned earlier, the suggested mechanisms behind the CDW transition are exciton condensation or a pseudo JT effect. Exciton formation occurs due to a weakly screened Coulomb interaction between the hole

pocket of the Se 4p band at Γ and the electron pocket of the Ti 3d band at L. In order for the hole and electron pockets to coincide in BZ the lattice periodicity must be doubled. Although evidence supports the existence of excitons in the $TiSe_2$ system, the CDW has been observed even when the excitons are suppressed by terahertz pulses[27].

Multiple models that consider a JT mechansim have been proposed for the $TiSe_2$ system. The model proposed by Hughes[5], for instance, suggests that the energy of a partially occupied d_{z^2} band is lower in a trigonal prismatic 2-H crystal field than in an octahedral 1-T field. In this model, the rotational modes of B-site Se about Ti leads to a configuration intermediate between the 2-H and 1-T polytypes.

The d electron occupancy of $TiSe_2$ is quite small and close to d^0 while the count in $TiTe_2$ is closer to $d^{\frac{1}{3}}$ as the size of Te atoms leads to greater chalcogen to transition metal charge transfer[28]. The Hughes model suggests an increase in charge transfer with Te doping initially leading to a more robust CDW. The suppression of the CDW with doping combined with no observation of the rotational modes in the local structure makes the Hughes mechanism unlikely.

The Whangbo[29] model, on the other hand, requires a JT driven CDW transition to shorten the Ti-Se bond length. This reduces the energy by delocalizing electrons and allows for hybridization between the Ti 3d and Se 4p orbitals. In this model, the p band is lowered and the transition does not rely on chalcogen to Ti charge transfer.

On the other hand, the Whangbo model can account for the dependence of the transition on Te doping. Consistent with our measurements, the trigonal phase is suppressed when Te is substituted into the lattice. Te disrupts the electronic homogeneity of the crystal and inhibits the cooperative JT observed in pure $TiSe_2$. A possible explanation for this is that Te orbitals are more diffuse[28] and Te atoms are heavier than Se, the energy gained through orbital overlap is diminished on the Ti-Te sites. As the Te electrons are more mobile, this may increase charge transfer to Ti d bands as the reduced p occupancy of the chalcogen sites leads to a weaker interaction.

Further evidence that would support that charge transfer suppresses the CDW comes from the monoclinic distortion above T_{CDW}. It is unusual for a high temperature phase to have lower symmetry than the low temperature phase. Despite this, the local structure analysis suggests that there is a monoclinic distortion of the local structure. $CrSe_2$ is a material that undergoes a similar phase transition[30]. $CrSe_2$ has a low temperature trigonal symmetry ($P\bar{3}m1$) with a monoclinic intermediate temperature phase (I2/m) that is caused by charge transfer to Cr leading to a degeneracy in the t_{2g} band that breaks the threefold rotation symmetry. In $TiSe_{2-x}Te_x$ this monoclinic distortion breaks up the long range order associated with the CDW. At low temperatures a cooperative JT effect drives orbital ordering that leads to a CDW phase. As the temperature increases above T_{CDW}, thermal fluctuations could lead to charge transfer on Ti. A degeneracy in the t_{2g} band of Ti can break the local C_3 symmetry while preserving the short range distortions, as observed in the local structure.

VI. ACKNOWLEDGEMENTS

The authors would like to thank Utpal Chatterjee for helpful discussions. The authors would like to thank Joerg Neuefeind, Craig Brown, and Keith Taddei for help carrying out the neutron diffraction experiments. The authors would like to acknowledge support from the Department of Energy DE-FG-02-01ER45927 We acknowledge the support of the National Institute of Standards and Technology, U.S. Department of Commerce, in providing the neutron research facilities used in this work. A portion of this research used resources at the High Flux Isotope Reactor and Spallation Neutron Source, a DOE Office of Science User Facility operated by the Oak Ridge National Laboratory.

[1] Y. Sun, S.-C. Wu, M. N. Ali, C. Felser, and B. Yan, Physical Review B **92**, 161107(R) (2015).
[2] K. T. Law and P. A. Lee, Proceedings of the National Academy of Sciences **114**, 6996 (2017).
[3] F. J. Di Salvo, D. E. Moncton, and J. V. Waszczak, Phys. Rev. B **14**, 4321 (1976).
[4] H. Cercellier, C. Monney, F. Clerc, C. Battaglia, L. Despont, M. G. Garnier, H. Beck, P. Aebi, L. Patthey, H. Berger, *et al.*, Physical review letters **99**, 146403 (2007).
[5] H. Hughes, Journal of Physics C: Solid State Physics **10**, L319 (1977).
[6] P. Goli, J. Khan, D. Wickramaratne, R. K. Lake, and A. A. Balandin, Nano letters **12**, 5941 (2012).
[7] K. Sugawara, Y. Nakata, R. Shimizu, P. Han, T. Hitosugi, T. Sato, and T. Takahashi, ACS nano **10**, 1341 (2015).
[8] P. Chen, Y.-H. Chan, X.-Y. Fang, Y. Zhang, M.-Y. Chou, S.-K. Mo, Z. Hussain, A.-V. Fedorov, and T.-C. Chiang, Nature communications **6** (2015).
[9] M. Noh, D. C. Johnson, and G. S. Elliott, Chemistry of materials **12**, 2894 (2000).
[10] A. F. Kusmartseva, B. Sipos, H. Berger, L. Forró, and E. Tutiš, Phys. Rev. Lett. **103**, 236401 (2009).
[11] E. Morosan, H. Zandbergen, B. Dennis, J. Bos, Y. Onose, T. Klimczuk, A. Ramirez, N. Ong, and R. Cava, Nature Physics **2**, 544 (2006).
[12] H. Luo, W. Xie, J. Tao, I. Pletikosic, T. Valla, G. S. Sahasrabudhe, G. Osterhoudt, E. Sutton, K. S. Burch, E. M. Seibel, *et al.*, Chemistry of Materials **28**, 1927 (2016).
[13] E. Morosan, K. E. Wagner, L. L. Zhao, Y. Hor, A. J. Williams, J. Tao, Y. Zhu, and R. J. Cava, Physical Review

B **81**, 094524 (2010).
[14] Y. Gu, Y. Katsura, T. Yoshino, H. Takagi, and K. Taniguchi, Scientific reports **5**, 12486 (2015).
[15] T. E. Kidd, T. Miller, M. Y. Chou, and T.-C. Chiang, Physical review letters **88**, 226402 (2002).
[16] G. Li, W. Z. Hu, D. Qian, D. Hsieh, M. Z. Hasan, E. Morosan, R. J. Cava, and N. L. Wang, Physical review letters **99**, 027404 (2007).
[17] M. Calandra and F. Mauri, Physical review letters **106**, 196406 (2011).
[18] C. Monney, H. Cercellier, F. Clerc, C. Battaglia, E. F. Schwier, C. Didiot, M. G. Garnier, H. Beck, P. Aebi, H. Berger, L. Forró, and L. Patthey, Phys. Rev. B **79**, 045116 (2009).
[19] A. Wegner, J. Zhao, J. Li, J. Yang, A. Anikin, G. Karapetrov, D. Louca, and U. Chatterjee, arXiv preprint arXiv:1807.05664 (2018).
[20] C. M. Fang, R. A. de Groot, and C. Haas, Phys. Rev. B **56**, 4455 (1997).
[21] T. Rohwer, S. Hellmann, M. Wiesenmayer, C. Sohrt, A. Stange, B. Slomski, A. Carr, Y. Liu, L. M. Avila, M. Kalläne, *et al.*, Nature **471**, 490 (2011).
[22] D. K. G. de Boer, C. F. van Bruggen, G. W. Bus, R. Coehoorn, C. Haas, G. A. Sawatzky, H. W. Myron, D. Norman, and H. Padmore, Phys. Rev. B **29**, 6797 (1984).
[23] D. K. G. deBoer, C. F. van Bruggen, G. W. Bus, R. Coehoorn, C. Haas, G. A. Sawatzky, H. W. Myron, D. Norman, and H. Padmore, Physical Review B **29**, 6797 (1984).
[24] B. E. Warren, *X-ray Diffraction* (Courier Corporation, 1990).
[25] D. L. Greenaway and R. Nitsche, Journal of Physics and Chemistry of Solids **26**, 1445 (1965).
[26] Y. Arnaud and M. Chevreton, Journal of Solid State Chemistry **39**, 230 (1981).
[27] M. Porer, U. Leierseder, J.-M. Ménard, H. Dachraoui, L. Mouchliadis, I. Perakis, U. Heinzmann, J. Demsar, K. Rossnagel, and R. Huber, Nature materials **13**, 857 (2014).
[28] E. Canadell, R. Brec, J. Rouxel, M.-H. Whangbo, *et al.*, Journal of solid state chemistry **99**, 189 (1992).
[29] M. H. Whangbo and E. Canadell, Journal of the American Chemical Society **114**, 9587 (1992).
[30] S. Kobayashi, H. Ueda, D. Nishio-Hamane, C. Michioka, and K. Yoshimura, Phys. Rev. B **89**, 054413 (2014).
[31] P. Peterson, M. Gutmann, T. Proffen, and S. Billinge, Journal of Applied Crystallography **33**, 1192 (2000).